J. Fluid Mech. (2003), *vol.* 481, *pp.* 67–76. © 2003 Cambridge University Press
DOI: 10.1017/S0022112003003768 Printed in the United Kingdom

A periodic-like solution in channel flow

By SADAYOSHI TOH[1] AND TOMOAKI ITANO[2]

[1]Department of Physics and Astronomy, Graduate School of Science, Kyoto University, Kyoto 606-8502, Japan

[2]Department of Aeronautics and Astronautics, Graduate School of Engineering, Kyoto University, Kyoto 606-8501, Japan

(Received 17 May 2002 and in revised form 26 December 2002)

We search channel flow for unsteady solutions for different Reynolds numbers and configurations by extending a shooting method which was previously used to obtain a travelling-wave solution. A general initial condition is considered. A periodic-like solution to the incompressible Navier–Stokes equations in a minimal flow unit is found. One cycle of the solution consists of two typical intervals: a single-streak period and a double-streak period. The solution seems to be periodic; however, it cannot be distinguished from a heteroclinic cycle which consists of two heteroclinic orbits connecting two single-streak solutions, because the solution is tracked only for one and half periods.

1. Introduction

The relationship between finite-amplitude and turbulent solutions in phase space has recently attracted attention through research on wall turbulence (see Nagata 1990; Ehrenstein & Koch 1991; Clever & Busse 1997; Waleffe 1998). Schmiegel (1999) suggested that the investigation of global bifurcations in phase space sheds some light on the mechanism of the transition from laminar to turbulent states. Recently, Kawahara & Kida (2001) educed a saddle-like periodic solution in Couette flow and found that it is embedded within a turbulent attractor. In research on Couette flow, we can expect that knowledge about finite-amplitude solutions will contribute much to the understanding of turbulence.

On the other hand, in the case of channel flow, the number of works on such solutions is still only a few (see Jiménez & Simens 2001; Waleffe 2001). Difficulties in finding such exact solutions directly and numerically result from the fact that turbulent channel flow has near-wall and outer regions; to describe many degrees of freedom contained in the outer region procedures to find solutions directly such as the Newton–Raphson method require high resolution, i.e. a large amount of computer resources. Besides, the accumulation of any digit errors will disturb the convergence of solutions significantly.

We adopted a different type of procedure to find a non-trivial solution, i.e. a travelling-wave solution (TWS) in our previous work (Itano & Toh 2001, hereafter referred to as IT01), which does not require such a large amount of computer resources but can only be applied to the case where a finite-amplitude solution has single unstable mode. In this paper, we shall extend the procedure and show a time-dependent solution obtained with it.

This solution appears to be a limit cycle in a phase space of channel flow, because the period of the solution converges with time. On the other hand, it has been shown

https://doi.org/10.1017/S0022112003003768 Published online by Cambridge University Press

(Holmes, Lumley & Berkooz 1996) that if a system has a special symmetry, $O(2)$, which corresponds to a reflection and translation symmetry in the spanwise direction in the case of channel flow, then a stable heteroclinic cycle can exist. In fact, our solution seems to be the heteroclinic cycle of a simplified model of near-wall turbulence introduced by Aubry *et al.* (1988). We, however, cannot determine whether the time-dependent solution is a limit cycle or a heteroclinic cycle because we tracked the solution only for one and half periods, which requires a large amount of CPU time. Therefore, we call our time-dependent solution a 'periodic-like' solution in this paper.

2. Numerical method

We will first address the numerical method to simulate channel flow. The incompressible Navier–Stokes equations are solved using the code of Kim, Moin & Moser (1987). Time marching is performed with a second-order Adams–Bashforth scheme for the convective terms and the Crank–Nicolson implicit scheme for the viscous terms. A Chebyshev-tau method in the wall-normal direction and a pseudo-spectral method in the streamwise and spanwise directions are used for spatial discretization. For dealiasing, the 1/2 phase shift scheme is adopted for both spatial discretizations. The flow field is expanded in 32×32 Fourier modes in the periodic directions (x: streamwise and z: spanwise) and 65 Chebyshev polynomials in the wall-normal direction (y: wall-normal). The no-slip boundary condition is imposed at the top ($y = +h$) and bottom ($y = -h$) walls, where h is the channel half-width.

Flow is driven by constant streamwise mass flux Q. We define the characteristic velocity U_c as $3Q/4h$; for laminar Poiseuille flow U_c is the centreline velocity. The Reynolds number based on U_c, h and the kinematic viscosity ν is kept constant at the value 3000. The friction Reynolds number $Re_\tau = u_\tau h/\nu$ is 130, where $u_\tau = \sqrt{\langle \partial_y u \rangle \nu}$ and $\langle \partial_y u \rangle$ is long-time-averaged velocity gradient on the walls. The streamwise and spanwise extents of the computational box are $L_x = \pi$ and $L_z = 0.4\pi$, respectively, or 420^+ and 170^+ in wall units. This system is a somewhat large 'minimal' flow unit, thus two pairs of high- and low-speed streaks, with spanwise extent less than 100^+ coexist frequently (see Jiménez & Moin 1991). In this sense, the system is in competition; the two pairs compete with each other. When one of the two defeats the other, the low-speed streak can develop strongly extending its height to the centre region.

Hereafter, we introduce several quantities to describe the state of channel flow. Quasi-two-dimensional (Q2D) and three-dimensional components of velocity are defined as $\boldsymbol{u}^{Q2D}(y,z,t) = (1/L_x)\int_0^{L_x} \boldsymbol{u}(\boldsymbol{x},t)\,\mathrm{d}x$ and $\boldsymbol{u}^{3D}(\boldsymbol{x},t) = \boldsymbol{u}(\boldsymbol{x},t) - \boldsymbol{u}^{Q2D}(y,z,t)$, respectively. Note that the Q2D component is not purely two-dimensional, because its streamwise velocity is not necessarily zero. Originally, this decomposition was proposed to study the self-sustaining process in plane Couette flow by Waleffe (1998). We also introduce the norm of each component of velocity per unit horizontal surface, defined as follows:

$$E_j(\boldsymbol{u}) = \frac{1}{hL_xL_z}\int_V [\boldsymbol{u}(\boldsymbol{x})]_j^2\,\mathrm{d}v, \tag{2.1}$$

where $j = x, y, z$, $\int_V(\cdot)\,\mathrm{d}v = \int_0^{L_x}\int_{-h}^{+h}\int_0^{L_z}(\cdot)\,\mathrm{d}x\,\mathrm{d}y\,\mathrm{d}z$ and $[\boldsymbol{v}]_j$ means the jth component of vector $\boldsymbol{v}$. We define unit energy and time as $E^\circ = U_c^2 h$ and $t^\circ = h/U_c$, respectively.

3. Procedure to educe finite-amplitude solutions

To obtain the unstable TWS, we have introduced a shooting method in which we adjust one parameter, the norm of the three-dimensional component of the initial

https://doi.org/10.1017/S0022112003003768 Published online by Cambridge University Press

condition. In this paper we search for a periodic solution by the shooting method; we try to keep the numerical solution close to a real periodic solution by adjusting the shooting parameter at the initial time. However, the original shooting method failed to solve for the periodic solution, because the period is quite long. Thus, we would require more than double precision to be used in the method. Here we improve the original shooting method by separating the total shooting period into intervals or substeps. In each interval, a separate shooting parameter is introduced and is adjusted to keep the numerical solution close to the relevant part of the periodic solution. In this sense, the numerically obtained solution is at most piecewise continuous.

The improved shooting method consists of the initial and shooting substeps. In the initial step, at the time $t = t_0$ we set the Q2D and three-dimensional velocity fields $\boldsymbol{u}_0^{Q2D}$ and $\boldsymbol{u}_0^{3D}$ to satisfy the following conditions:

$$\nabla \cdot \boldsymbol{u}_0^{Q2D} = \nabla \cdot \boldsymbol{u}_0^{3D} = 0, \tag{3.1}$$

$$\frac{1}{L_z}\int_{-h}^{+h}\int_0^{L_z} \left[\boldsymbol{u}_0^{Q2D}\right]_x \mathrm{d}y\,\mathrm{d}z = Q, \tag{3.2}$$

$$\boldsymbol{u}_0^{Q2D}(\boldsymbol{x}) = \boldsymbol{u}_0^{3D}(\boldsymbol{x}) = \boldsymbol{0} \quad \text{at} \quad y = \pm h. \tag{3.3}$$

In the ith shooting substep ($i = 1, 2, \ldots$), at the starting time t_{i-1} the initial condition $\boldsymbol{u}_i(\boldsymbol{x}, t_{i-1})$ is set using the velocity field obtained at the time t_{i-1} in the former step, $\boldsymbol{u}_{i-1}(\boldsymbol{x}, t_{i-1})$ as follows:

$$\boldsymbol{u}(\boldsymbol{x}, t_{i-1}) = \boldsymbol{u}_{i-1}^{Q2D}(\boldsymbol{x}, t_{i-1}) + f_i \boldsymbol{u}_{i-1}^{3D}(\boldsymbol{x}, t_{i-1}), \tag{3.4}$$

where f_i is the ith shooting parameter, and $\boldsymbol{u}_{i-1}^{Q2D}(\boldsymbol{x}, t_{i-1})$ and $\boldsymbol{u}_{i-1}^{3D}(\boldsymbol{x}, t_{i-1})$ are the Q2D and three-dimensional components of $\boldsymbol{u}_{i-1}(\boldsymbol{x}, t_{i-1})$. Then, by means of DNS, we advance the flow field $\boldsymbol{u}(\boldsymbol{x}, t)$ until $t = t_i$ from the initial field $\boldsymbol{u}(\boldsymbol{x}, t_{i-1})$.

Here, the fitting parameter f_i is determined as $\boldsymbol{u}_i(\boldsymbol{x}, t)$ is kept on the basin boundary of the turbulent state for $t_{i-1} \leqslant t < t_i$. Henceforth, we denote the basin boundary by $\mathscr{B}$. For almost all the values of f_i, the solution eventually reaches either the laminar or turbulent state. Thus the periodic solution on $\mathscr{B}$ seems to be hyperbolic in the whole phase space, while it is stable on $\mathscr{B}$. The interval $t_i - t_{i-1}$ is selected so that the parameter f_i is determined up to 13 decimal places and the solution $\boldsymbol{u}_i$ is converged in this interval. In fact, we have taken f_i to satisfy the following condition by advancing the flow until $t = t_i + \delta t$:

$$E_l < E_y(\boldsymbol{u}^{3D}(t_i + \delta t)) < E_t, \tag{3.5}$$

where δt is set to be much larger than the time scale on which solutions escape from $\mathscr{B}$ (see figure 1). The constants E_l and E_t are the thresholds of E_y for the escape of the numerical solution to the laminar and the turbulent states respectively. In the present simulation, $E_y(\boldsymbol{u}^{3D})$ is numerically less than 10^{-14} for the laminar state, while it fluctuates around 10^{-3} for the turbulent state. Therefore, in this paper, we set $E_l = 2 \times 10^{-7} E^\circ$, $E_t = 2 \times 10^{-5} E^\circ$, and $\delta t = 200 t^\circ$. This procedure guarantees that the solution is kept close to the real solution at least for $t_{i-1} \leqslant t \leqslant t_i$.

As initial velocity fields for the initial step, we adopt the following:

$$\left[\boldsymbol{u}_0^{Q2D}(\boldsymbol{x})\right] = \left(1 - y^2, -\frac{\partial \Psi}{\partial z}, \frac{\partial \Psi}{\partial y}\right), \qquad \left[\boldsymbol{u}_0^{3D}(\boldsymbol{x})\right] = \left(0, 0, -\frac{\partial \Phi}{\partial y}\right), \tag{3.6}$$

where $\Psi(y, z) = F(y)\sin(2\pi z/L_z)$, $\Phi(x, y) = F(y)\sin(2\pi x/L_x)$ and $F(y) = A(\exp(c_m(-y-1))-1)^2(\exp(c_p(y-1))-1)^2$. Hereafter we use $A = 1 \times 10^{-10}$, $c_m = 1$,

https://doi.org/10.1017/S0022112003003768 Published online by Cambridge University Press

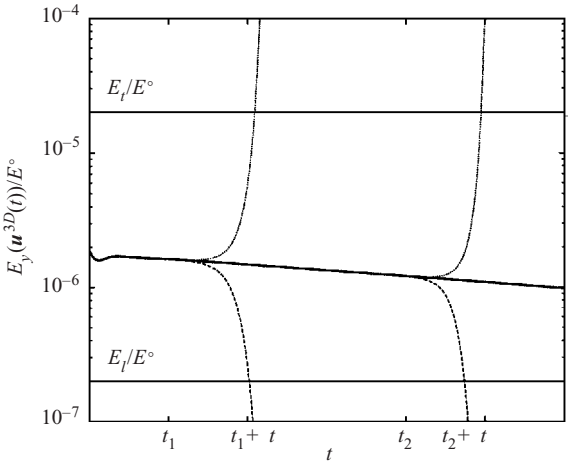


FIGURE 1. Typical trajectories in the first and second shooting substeps. The dotted and dashed lines at each step are the trajectories obtained with f_i slightly larger and smaller than that of the finally obtained solution (the thick line) which is also superimposed for reference. The lines labelled E_t/E° and E_l/E° indicate the thresholds for detecting the escape of a solution to the turbulent and laminar states, resepctively.

$c_p = -6$. The Q2D field $\boldsymbol{u}_0^{Q2D}$ consists of laminar Poiseuille flow and a vortex pair of streamwise vorticity with positive and negative sign. Their vorticity is approximately localized around $y \approx -0.8h$. At the early stage, they are dissipated by viscosity while a single low-speed streak is produced (at $z \approx L_z/2$) between the vortex pair. On the other hand, the three-dimensional field $\boldsymbol{u}_0^{3D}$ plays the role of an initial disturbance which keeps $\boldsymbol{u}(t)$ from being attracted to the laminar state in the shooting substeps.

Although we assume that the subsequent fragmentary solutions obtained in each substep are connected at $t = t_i$ $(i = 0, 1, \ldots)$, the overall solution is not a 'solution' governed by the Navier–Stokes equations in the strict sense because of its discontinuity. However, we consider that an exact solution exists on $\mathscr{B}$ and can be approximated by our piecewise continuous solution. This is illustrated in a schematic view (figure 2). The fact that f_i nearly equals 1 for $i \geqslant 2$ (see table 1) suggests that the exact solution can be approximated by our solution with reasonable accuracy. Hereafter, this piecewise continuous solution is referred as the 'chain solution'. The chain solution consists of several 'chains', i.e. its parts solved in the shooting substeps. It is noted that the phase space is not as simple as in figure 2 because the dimension of the real phase space is comparable to the number of effective degrees of freedom used in DNS.

4. Results

We first examine the evolution of the energy input and output of the channel. The energy equation for channel flow is

$$\frac{\mathrm{d}E}{\mathrm{d}t} = F - D, \tag{4.1}$$

where

$$E = \frac{1}{2hL_xL_z}\int_V \|\boldsymbol{u}\|^2\,\mathrm{d}v, \quad F = \frac{-1}{hL_xL_z}\int_V \frac{\partial p u_x}{\partial x}\,\mathrm{d}v, \quad D = \frac{1}{hL_xL_z}\int_V \nu\|\boldsymbol{\omega}\|^2\,\mathrm{d}v.$$

https://doi.org/10.1017/S0022112003003768 Published online by Cambridge University Press

i	t_i/t°	t_{i+1}/t°	f_i
1	0	400	0.1923084300000
2	400	1000	0.9976730218680
3	1000	1600	0.9995608923211
4	1600	2200	0.9997185682085
5	2200	2800	0.9999493218349
6	2800	3400	0.9970611283536
7	3400	4000	0.9999113533069
8	4000	4600	0.9994596024291
9	4600	5100	0.9971752409579
10	5100	5700	0.9999670511936

TABLE 1. f_i at the ith step.

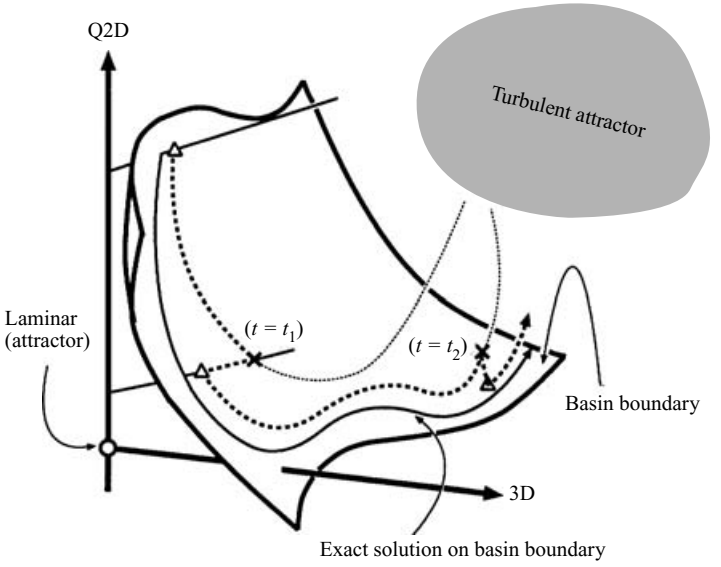


FIGURE 2. Schematic view of the phase space in which we obtained a periodic-like solution. The factor f_i of the three-dimensional velocity component of the chain solution (thick dashed line) is adjusted at $t = t_i (i = 1, 2, \ldots)$ so that it is close to an exact solution (solid line) on the basin boundary between the laminar and turbulent attractors. As a result, we find that this exact solution shows a kind of periodicity.

Figure 3 shows the evolution of $\mathrm{d}E/\mathrm{d}t$ of the chain solution, where the ten chains are represented by different types of lines. It is easy to see that the intervals for $F < D$ are shorter than those for $F > D$; the kinetic energy of the system is dissipated quickly in the former, while it is recovered gradually in the latter. For convenience, we label six intervals in which $\mathrm{d}E/\mathrm{d}t$ is positive: T_1 for $423 < t/t^\circ < 1914$, T_2 for $2012 < t/t^\circ < 2089$, T_3 for $2491 < t/t^\circ < 3633$, T_4 for $3730 < t/t^\circ < 3807$, T_5 for $4209 < t/t^\circ < 5350$, and T_6 for $5448 < t/t^\circ < 5525$.

Note that two peaks seen in T_2, T_4 and T_6 in the figure are strikingly similar. This similarity suggests that the chain solution is attracted towards a periodic solution as time increases. In order to make the periodicity of the chain solution clearer, we show the evolution in the (F, D)-plane in figure 4. In the figure, the chain solution orbits in the clockwise direction with time, travelling through more than two orbits. It

https://doi.org/10.1017/S0022112003003768 Published online by Cambridge University Press

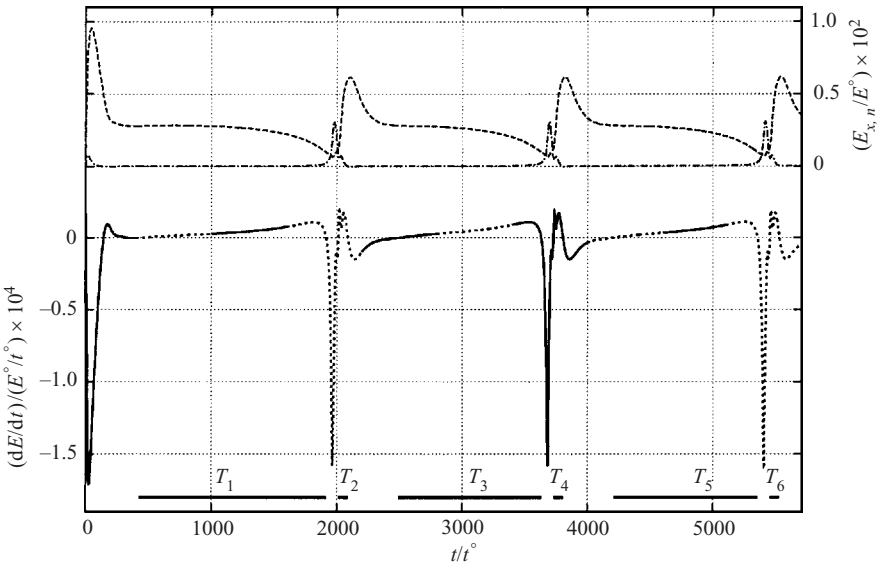


FIGURE 3. Evolution of $\mathrm{d}E/\mathrm{d}t$ (thick solid and thick dashed lines) and $E_{x,n}$ $(n = 1, 2)$ (long-dashed and dash-dotted lines) for the chain solution. Line type for $\mathrm{d}E/\mathrm{d}t$ is changed at the discontinuous times $t_i (i = 1, 2, \ldots)$. The thick horizontal lines labelled T_i indicate the periods in which $\mathrm{d}E/\mathrm{d}t$ is positive.

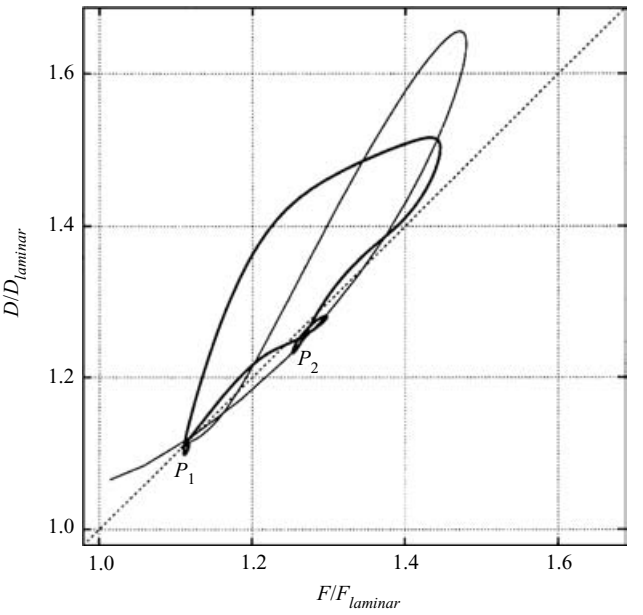


FIGURE 4. Plot of the trajectory of the chain solution on the (F, D)-plane normalized by their laminar values; solid line: transient time $0 < t/t^\circ < 423$, thick solid line: close to periodic solution $423 < t/t^\circ < 4600$. Dashed line corresponds to $F/F_{laminar} = D/D_{laminar}$. $F_{laminar}$ and $D_{laminar}$ are the energy input and dissipation of laminar Poiseuille flow, respectively.

https://doi.org/10.1017/S0022112003003768 Published online by Cambridge University Press

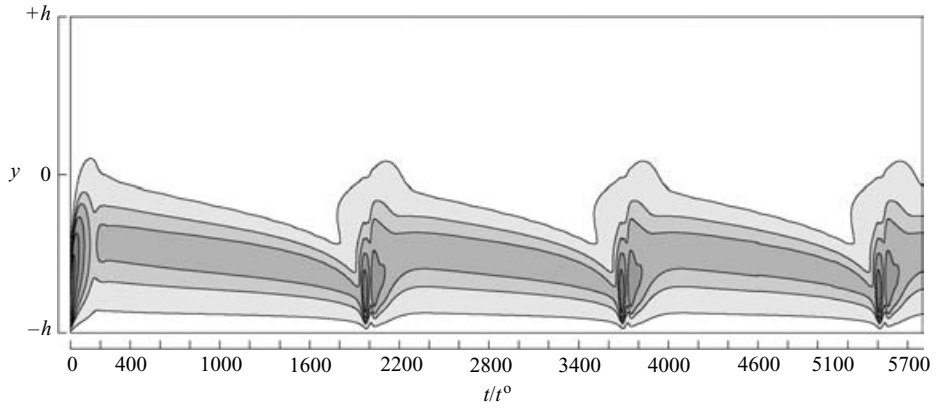


FIGURE 5. Evolution of Reynolds stress in the chain solution. Shaded region indicates $\langle uv\rangle(y,t) < -0.0001$. $\langle uv\rangle$ varies from -0.0029 to 0.00001. Contour levels are -0.0001, -0.0002, -0.0004, -0.0008, -0.0016, -0.0032, -0.0064, -0.0128, -0.0256.

should be noted that the solution's speed around the orbit is not constant. In fact, the chain solution spends a relatively long time near the two typical points, P_1 and P_2 in figure 4. These two points in the (F, D)-plane correspond to two kinds of relatively steady states in the physical space: single-streak and double-streak states respectively, which will be described later in this section.

An analysis of Reynolds stress provides further evidence for the periodicity of the chain solution (see figure 5). Reynolds stress gives a measure of the momentum flux due to the turbulence in the channel. We define Reynolds stress integrated over the horizontal plane, as follows:

$$\langle uv\rangle(y,t) = \frac{1}{L_x L_z}\int_0^{L_x}\int_0^{L_z} [\boldsymbol{u}(\boldsymbol{x},t)]_x [\boldsymbol{u}(\boldsymbol{x},t)]_y \,\mathrm{d}x\,\mathrm{d}z, \tag{4.2}$$

which is henceforth referred to as Reynolds stress in this paper. It seems that, in intervals such as $F < D$, the large amount of energy dissipation is associated with the sudden increase of Reynolds stress in the lower region $-h < y < 0$.

Next, we confirm the closeness of the chain solution to a periodic solution. In the physical space, the periodic solution can travel in both x- and z-directions in each period. The phase velocities c_x and c_z of the TWS obtained in IT01 have been estimated as $c_x \approx 0.7U_c$ and $c_z \approx 0.001U_c$. Such a translational invariance could make the confirmation of the periodicity in the phase space difficult. Accordingly, we numerically estimate the translation vector in the horizontal plane, $\delta\boldsymbol{x} = \delta x\boldsymbol{e}_x + \delta z\boldsymbol{e}_z$, that minimizes the norm E_j of the difference field, defined as follows:

$$\delta\boldsymbol{u}(t_1,t_2,\boldsymbol{x},\delta\boldsymbol{x}) = \boldsymbol{u}(t_1,\boldsymbol{x}) - \boldsymbol{u}(t_2,\boldsymbol{x}-\delta\boldsymbol{x}). \tag{4.3}$$

Moreover, to evaluate the difference, we introduce the relative error

$$\hat{E}_j(t_1,t_2) = \frac{\min_{\delta x,\delta z} E_j(\delta\boldsymbol{u}(\boldsymbol{x},\delta\boldsymbol{x},t_1,t_2))}{E_j(\boldsymbol{u}(\boldsymbol{x},t_1))} \tag{4.4}$$

for $j = x, y, z$. We calculate $\hat{E}_y$ of the difference field between the velocity field at two times separated by half a period, about $1700t^\circ$. For $t_1 = 2500.00t^\circ$ and $t_2 = 4191.61t^\circ$, the minimum relative error is obtained for $(\delta x, \delta z) = (0.383060L_x, 0.500000L_z)$: $\hat{E}_y = 7\times10^{-7}$. Within this numerical accuracy, we conclude that the chain solution

https://doi.org/10.1017/S0022112003003768 Published online by Cambridge University Press

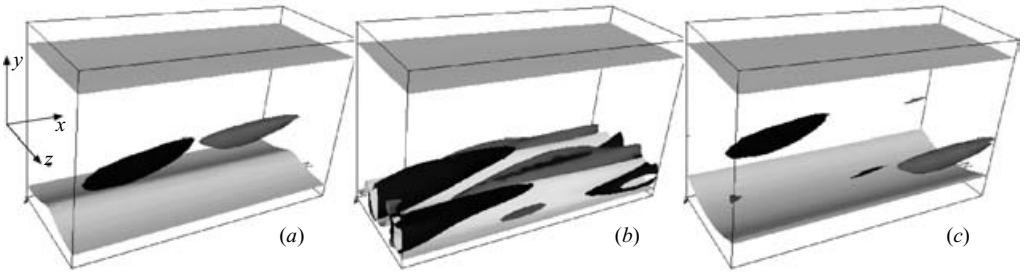


FIGURE 6. Snapshots of the streamwise vortex and streak in the whole channel at typical times (*a*) $t = 800t^\circ$ in T_1, (*b*) $t = 1990t^\circ$ between T_1 and T_3, (*c*) $t = 2500t^\circ$ in T_3. Light grey isosurfaces represent $[u]_x/U_c = 0.4$. Quasi-streamwise vortices with positive (black) and negative (grey) streamwise vorticity are represented by isosurfaces of $Q/((U_c/h)^2) = 0.005$. The second invariant Q is defined as $\frac{1}{2}\sum_{i,j}(W_{ij}W_{ij} - S_{ij}S_{ij})$, where S_{ij} and W_{ij} are symmetric and antisymmetric parts of the velocity gradient tensor $\partial u_i/\partial x_j$, respectively.

is periodic, taking the translational invariance into account. Because the function travels in the streamwise direction without much change in its form over a relatively long time, δx continuously increases as t_2 increases. On the other hand, δz is almost equal to $L_z/2$ and we find that this value is the same for t_2 in both of the intervals T_1 and T_5. We have also calculated the minimum of the difference between the fields at $t_1 = 2500.00t^\circ$ and $t_2 \approx 800t^\circ$. In this case, the relative error, $\hat{E}_y$, is of order 10^{-4} and $\delta z = 0.500001L_z$. This suggests that the chain solution gets close to the periodic solution as the number of the shooting substeps increases. Note that the solutions at the three times considered above, $t = 800.00t^\circ$, $2500.00t^\circ$ and $4191.61t^\circ$ differ only in phase in the z-direction by π; the solutions at $t = 800.00t^\circ$ and $t = 4191.61t^\circ$ are the same but the solution at $t = 2500.00t^\circ$ is shifted by π in z. This means that the periodic solution consist of two cycles that differ in the phase of z by π.

Next, we focus on the temporal evolution of the chain solution in the physical space. One of the most interesting characteristics of the present chain solution is the evolution of the number of "streaks", which emerge only near the lower wall. Streaks and quasi-streamwise vortices are typical coherent structures in wall turbulence, which are often defined by some ensemble-averaging method in experimental or numerical studies (see Schoppa & Hussain 2002). Streaks correspond to low-speed regions elongated in the streamwise direction. They are often observed to be flanked by staggered vortices riding over them. Since these vortices are dominated by streamwise vorticity, they are called quasi-streamwise vortices.

In the intervals T_1, T_3 and T_5, both a single (low-speed) streak and a single pair of quasi-streamwise vortices with positive and negative vorticity are found in the lower region $-h < y < 0$ (see figure 6*a*, *c*). As mentioned above, the streak and vortex pair in T_3 are shifted by half in z relative to those in T_1 and T_5. These coherent states travel downstream with almost constant speed without changing their shapes significantly. In fact, the typical time scale of a bursting process in the turbulent state is $O(10t^\circ)$, which is far shorter than the period of the chain solution. On the other hand, around T_2, T_4 and T_6, we can find two definite streaks and two pairs of quasi-streamwise vortices (see figure 6*b*). Figure 3 displays the evolution of $E_{x,1}$ and $E_{x,2}$, which are the energies of the modes with $k_z = 1$ and $k_z = 2$, and defined as follows:

$$E_{x,n} = \frac{1}{hL_xL_z}\int_V \left|[\boldsymbol{u}]_x^{k_z=2\pi n/L_z}\right|^2 \mathrm{d}v. \tag{4.5}$$

https://doi.org/10.1017/S0022112003003768 Published online by Cambridge University Press

In a relatively small domain such as the present minimal flow, the number of dominant streaks is closely related to the suffix n of the dominant mode energy, $E_{x,n}$. Additionally, the contribution of the upper region $0 < y < +h$ to $E_{x,n}$ is smaller than that of the lower region, because there is no structure in the upper region. Therefore, a comparison among $E_{x,n}$ shows the change of the number of streaks in the lower region. From figure 3, we can roughly but quantitatively see that two streaks coexist in T_2, T_4 and T_6, while one streak exists in T_1, T_3 and T_5.

5. Concluding remarks

We have obtained a periodic-like solution using an extended shooting method. Although the solution is piecewise continuous, we have confirmed that the periodicity holds to within a $10^{-2}\%$ relative error. This periodic-like solution consists of a single-streak state and a double-streak state; the former seems to correspond to a saddle point, strictly speaking a travelling wave. Moreover, there exist two single-streak states that differ only in phase in the z-direction by π. This means that the periodic-like solution goes through single-streak states twice before it closes its period, that is, in figure 4 only half of the period is shown.

It is interesting that our periodic-like solution is similar to a heteroclinic cycle obtained by means of a simplified model of near-wall turbulence by Aubry *et al.* (1988), although their approach is completely different from ours. Their cycle connects two fixed points which correspond to quiescent streak states, and differ only in the phase of z by half a wavelength in real space, like our single-streak solutions. As mentioned in the Introduction, a reflection and translation symmetry in the spanwise directiction, which holds in channel flow, makes a heteroclinic cycle structurally stable. Although a heteroclinic cycle has an infinite period, any piecewise approximation to it, like ours, would have an apparent period depending entirely on the approximation error. Of course, even if a system has this symmetry, a heteroclinic cycle can still be structurally unstable and a periodic solution, which might be close to the heteroclinic cycle, can emerge through a global bifurcation. Thus, we cannot conclude whether the periodic-like solution is a heteroclinic cycle or an exact periodic solution. Indeed, in both cases, the two single-streak states might be saddle points, even on $\mathscr{B}$.

We cannot find these saddle points by means of our shooting method, because disturbances in two unstable directions cannot be removed by one shooting parameter. The single-streak state closely resembles the TWS obtained in IT01. We have inferred that since the TWS is a saddle point and stable on $\mathscr{B}$, it can be obtained by the shooting method. However, we note that in IT01 the TWS was calculated using a shooting method on just a single time interval. The computational restrictions this method imposes may not allow us to conclude convergence to the TWS. To confirm the existence of the TWS, we applied the present procedure to the TWS obtained in IT01. Within the first three shooting substeps, it was observed that the single-streak state regarded as the TWS goes through the double-streak state to the other single-streak state, and that the flow loses a spanwise drift. Thus it is probable that in IT01 we have found part of the periodic-like solution and regarded it as the TWS.

The initial condition (3.6) is quite general and can be applied to different configurations and Reynolds numbers, because it does not depend directly on any DNS data. Initial conditions should be close enough to the basin boundary of the turbulent attractor, and also in the basin of the solution that will be shot. In IT01 we selected one snapshot satisfying such conditions through a long time series, which may not be efficient when we try to find solutions in other cases. The flow field

https://doi.org/10.1017/S0022112003003768 Published online by Cambridge University Press

(3.6) consists of the laminar Poiseuille flow, one streamwise vortex pair and the three-dimensional disturbance. This flow is enough to create a single Q2D streak that develops into one of the TWS or periodic-like solutions associated with TWS through three-dimensional instability on the basin boundary of the turbulent attractor. We are trying to find such solutions for several Reynolds numbers.

The escape processes from the single-streak and double-streak states are quite similar to bursting processes observed in real turbulence as seen in the evolution of the Reynolds stress. In real turbulence, as discussed in IT01, an orbit would go close to the basin boundary of the turbulent attractor along the stable manifold of the periodic-like solution and then escape along the unstable one. This suggests that the bursting process can be understood by examining the periodic-like solution. Moreover, the recursive nature of the bursting process may also be explained qualitatively. However, the periodic-like solution is confined in the inner layer without exciting the outer layer. We infer that the inner and outer layers are separated dynamically, and some coupling mechanism is required to sustain turbulence in the outer layer. We intend to investigate this issue further in the future.

This work has been partially supported by Grant-in-Aid for Science Research on Priority Areas (B) from the Ministry of Education, Culture, Sports, Science and Technology of Japan. The authors would like to express their cordial thanks to Dr D. P. Wall for improving the manuscript.

REFERENCES

Aubry, N., Holmes, P., Lumley, J. L. & Stone, E. 1988 The dynamics of coherent structures in the wall region of a turbulent boundary layer. *J. Fluid Mech.* **192**, 115–173.

Clever, R. M. & Busse, F. H. 1997 Tertiary and quaternary solutions for plane Couette flow. *J. Fluid Mech.* **344**, 137–153.

Ehrenstein, U. & Koch, W. 1991 Three-dimensional wavelike equilibrium states in plane Poiseuille flow. *J. Fluid Mech.* **228**, 111–148.

Holmes, P., Lumley, J. L. & Berkooz, G. 1996 *Turbulence, Coherent Structures, Dynamical Systems and Symmetry*. Cambridge University Press.

Itano, T. & Toh, S. 2001 The dynamics of bursting process in wall turbulence. *J. Phys. Soc. Japan* **70**, 703–716 (referred to herein as IT01).

Jiménez, J. & Moin, P. 1991 The minimal flow unit in near-wall turbulence *J. Fluid Mech.* **225**, 213–240.

Jiménez, J. & Simens, M. P. 2001 Low-dimensional dynamics of a turbulent wall flow. *J. Fluid Mech.* **435**, 81–91.

Kawahara, G. & Kida, S. 2001 Periodic motion embedded in plane Couette turbulence: regeneration cycle and burst. *J. Fluid Mech.* **449**, 291–300.

Kim, J., Moin, P. & Moser, R. 1987 Turbulence statistics in fully developed channel flow at low Reynolds number. *J. Fluid Mech.* **177**, 133–166.

Nagata, M. 1990 Three-dimensional finite-amplitude solutions in plane Couette flow: bifurcation from infinity. *J. Fluid Mech.* **217**, 519–527.

Schmiegel, A. 1999 Transition to turbulence in linearly stable shear flows. PhD thesis, Philipps-Universität, Marburg.

Schoppa, W. & Hussain, F. 2002 Coherent structure generation in near-wall turbulence. *J. Fluid Mech.* **453**, 57–108.

Waleffe, F. 1998 Three-dimensional coherent states in plane shear flows. *Phys. Rev. Lett.* **81**, 4140–4143.

Waleffe, F. 2001 Exact coherent structures in channel flow. *J. Fluid Mech.* **435**, 93–102.

https://doi.org/10.1017/S0022112003003768 Published online by Cambridge University Press